Research Article

Equilibrium and kinetic studies on adsorption of chromium(VI) onto pine-needle-generated activated carbon

George M. Ayoub[1] · Ahmad Damaj[1] · Houssam El-Rassy[2] · Mahmoud Al-Hindi[3] · Ramez M. Zayyat[1]

Received: 29 July 2019 / Accepted: 1 November 2019 / Published online: 6 November 2019

Abstract
Chromium is extensively used in a large number of industries and is often discharged through the wastewater effluents to pollute water sources. Being a heavy metal, it invariably leads to serious health risks when ingested. The aim of the present study is to test a readily available low-cost precursor, dry pine needles, for the production of activated carbon and determine its efficiency in removing Cr(VI) from water. Process parameters such as efficiency of metal removal, capacity of the activated carbon, pH, and concentration of adsorbate were investigated. The characterization of the adsorbent was performed using scanning electron microscopy and X-ray diffraction. The point of zero charge was determined. Both batch and column adsorption experiments were conducted. Adsorption equilibrium isotherms as well as adsorption kinetics were generated from batch experiments. Breakthrough curves were generated to assess adsorption capacities using column adsorption tests. The results obtained from the batch tests showed that the Freundlich as well as Temkin isotherms constituted a better fit for the adsorption data than the Langmuir isotherm. Maximum adsorption capacity of pine-needle activated carbon for Cr(VI) was 65.36 mg g^{-1}. Furthermore, the adsorption kinetics followed a pseudo-second order which confirms chemisorption to be the mechanism responsible for the removal of Cr(VI) using pine-needle activated carbon as adsorbent. The results of the column tests indicated that the highest metal removals were achieved at lower initial concentrations, while the highest adsorption capacities were achieved at the initial concentration of 20 mg L^{-1}. The results also depicted that Cr(VI) is almost exclusively removed at low pH values (pH 4 being the lowest pH tested) with removals decreasing appreciably with the increase in pH.

Keywords Activated carbon · Pine needles · Hexavalent chromium · Isotherms · Kinetics

1 Introduction

Chromium is one of the widely used metals in industries such as leather tanning, electroplating, metal finishing, textile finishing, steel fabrication, wood preservation and pulp processing, paint, dyes, paper, fertilizers, and photography [1–5]. It is normally released in industrial effluents and exists in the stable oxidation states of trivalent chromium, Cr(III), and hexavalent chromium, Cr(VI), where the latter is primarily present in the form of chromate ($HCrO_4^-$) and dichromate ($Cr_2O_7^{2-}$) ions which are established to be highly toxic metals to humans and animals [6–8]. Discharges of such effluents to water sources, particularly in developing countries where treatment of industrial wastewater is rather limited, invariably lead to health risks which include ailments such as dermatitis,

Electronic supplementary material The online version of this article (https://doi.org/10.1007/s42452-019-1617-7) contains supplementary material, which is available to authorized users.

✉ George M. Ayoub, gayoub@aub.edu.lb | [1]Department of Civil and Environmental Engineering, American University of Beirut, Beirut, Lebanon. [2]Department of Chemistry, American University of Beirut, Beirut, Lebanon. [3]Baha and Walid Bassatne Department of Chemical Engineering and Advanced Energy, American University of Beirut, Beirut, Lebanon.

allergic skin reactions, ulceration of the intestines, bronchitis, cancer of the digestive system, and lungs and may cause other health problems such as perforation of the nasal septum, severe diarrhea, and hemorrhaging [9–11]. It should be noted that maximum permissible levels for Cr(VI) in water vary from country to another and, as per the Lebanese standards, the maximum permissible limits for Cr(VI) discharges in water destined for potable use are 0.05 mg/L [12, 13].

In order to alleviate this serious concern and to comply with the set limits, processes such as chemical precipitation, ion exchange, adsorption, biosorption, co-precipitation, electrodialysis, membrane filtration, reverse osmosis, and solvent extraction have been employed to investigate the removal of Cr(VI) from aqueous solutions [14–16]. A number of these processes are deemed unsustainable because of a number of disadvantages such as being relatively expensive with high operating cost due to excessive energy consumption, having low selectivity and high sludge production, and inducing incomplete removal of the targeted metal ions [17–19]. Adsorption methods using activated carbon are considered by many to be the most favorable technique for metal removal; however, the costs involved in its production and generation pose some hindrance to its use [20, 21]. Several production processes were investigated to produce ACs using precursors that are cheaply and abundantly available and thus more sustainable. Some of the precursors, such as pecan shells [22], olive-waste cakes [23], fertilizer industrial waste [18], pine cones [24], rice husks [25], are reported to have been successfully tested after activation for the removal of metals from aqueous solutions.

In this study, dry pine needles are selected as a precursor for the production of AC due to a number of inducing factors. Pine trees are very common in Lebanon whereby they constitute most of the forests which occupy an area of approximately 17,000 ha. Massive amounts of pine needles are shed yearly, which if left unmanaged would constitute fire and health hazards provoked by their highly inflammable and slippery characteristics when present in the dry form. Considering the ease by which this organic-based material could be collected, handled, and converted into AC renders this precursor a potentially viable and sustainable material source for the production of a commercial entity, while concurrently alleviating possible environmental risks.

The objective of the present study is to determine the efficacy of dry pine needles, as a low-cost precursor for the production of AC, in the removal of Cr(VI) from aqueous solutions. Characterization of the activated carbon adsorbent is performed. Batch experiments are conducted to determine the adsorption equilibrium isotherms as well as kinetic aspects. Column studies are performed to establish the efficiency of metal removal, capacity of the AC, optimum pH, and concentration of adsorbate.

2 Materials and methods

2.1 Preparation and characterization of the AC

Shed dry pine needles of the type *Pinus pinea* were collected from the campus of the American University of Beirut and used as a precursor for producing activated carbon. The procedure for the preparation of the AC involved, in a first step, chemical activation of the washed, dried, and crushed needles by impregnating in KOH for a period of 24 h. The impregnation was carried out using 1.0 g of KOH(1 M) per gram of biomass. This was followed by drying the activated needles at 120 °C for a 24 h period. The resulting activated pine needles were then placed in high-temperature-resisting porcelain crucibles and were carbonized in a in an oven operated under inert conditions created by the addition of nitrogen at a rate of 500–700 mL min^{-1}. Application of heat was conducted at a rate of 10 °C min^{-1} until the target temperature of 800 °C was attained. After 1 h of carbonization, the product was left to cool for several hours while maintaining the flow of nitrogen in the oven. The produced carbon was washed with boiling water, filtered, and then rewashed with a small volume of 5 M HCl. Any free acid left on the AC was carefully washed using distilled water then dried at 105 °C and crushed to produce granular AC. The product was placed in vials which were stored in a desiccator for ultimate use in the experimental study.

Derivative thermogravimetry (DTG) and thermogravimetric analysis were performed (TGA). The AC samples were analyzed by X-ray diffraction on a Brucker D8 ADVANCE X-ray diffractometer equipped with a Cu-Kα radiation source (Figure S1). Scanning electron microscopy (SEM) was performed on samples of the activated carbon using a TESCAN MIRA3 LMU scanning electron microscope. Thermo-Finnigan Flash EA series 1112 was used to determine the elemental analysis of raw pine needles and AC pine needles. Sodium, potassium, and silica were determined using ICP-OES Shimadzu 9800 series, following microwave-assisted digestion.

Determining the classes of functional groups present on the surface of the AC is a good indicator of the adsorption mechanisms taking place on the surface of the adsorbent. In this context, KBr pellets with a 0.5% content of pine-needle AC were prepared and tested using Fourier transform infrared (FT-IR) spectroscopy on a Nicolet™ 4700 FTIR spectrometer.

For further characterization, the point of zero charge (PZC) of the pine-needle AC was determined. At the PZC of

the AC, the total charge of the surface functional groups is equal to zero. If the pH of a solution is above its PZC, the AC surface will have a net negative charge and predominantly exhibit an ability to exchange cations, while the AC will mainly retain anions if the solution pH is below its PZC [26]. The PZC was determined by adding 0.1 g of the AC to solutions of NaCl at different pH values. The solution that will not show a change in pH after 24 h from the addition of AC is considered to have the closest pH to the PZC of the AC.

2.2 Column adsorption tests

Fixed-bed adsorption column tests were conducted to determine the efficiency of the pine-needle AC in removing chromium.

To calculate the amount of Cr(VI) adsorbed per unit mass of adsorbent, the following mass balance equation was used:

$$q_e = \frac{(C_0 - C_e)V}{m} \quad (1)$$

where q_e is the amount of Cr(VI) adsorbed at equilibrium (mg g^{-1}), C_0 is the initial concentration of Cr(VI) (mg L^{-1}), C_e is the final Cr(VI) concentration at equilibrium (mg L^{-1}), V is the volume of water treated (L), and m is the mass of adsorbent (g), while the % removal of Cr(VI) was calculated as follows:

$$\%\text{Cr(VI) removal} = \frac{(C_0 - C_e)100}{C_0}. \quad (2)$$

The fixed-bed tests were conducted using a set of two plexi-glass columns, 2.3 cm internal diameter and 15 cm long, installed on a stand and packed with thoroughly mixed batches of AC to ensure uniformity in bed composition. Prior to loading each column with 2 g of AC, the columns were packed with glass wool for a depth of 1 cm to ensure that the granular AC will not escape from the column. The AC was also boiled in water for a period of 10 min so that all air trapped inside the AC pores will be replaced by water (ASTM method D6586). Acid wash was applied to the columns after each test.

A set of two master flex peristaltic pumps supplied by Cole-Parmer, USA was used to feed the water/metal solution at a constant flow rate to the top of the column to allow for gravity flow through the column. The flow rate to the columns was fixed at 15 mL min^{-1}.

Testing procedures involved the preparation of 300 mg L^{-1} stock solutions of the metals using deionized (DI) water and the salt of the metal ($K_2Cr_2O_7$). Adjustments to the water/metal pH solutions, where needed, were performed through the addition of 0.5 M HCl or 0.5 M NaOH while constantly measuring the influent metal concentration after arriving at a fixed pH value. Periodic sampling of the effluent was carried out at periods ranging from 1 min to 30 min depending on the metal adsorption rate.

Standard methods were adopted in the analytical testing procedures of pH and metal concentrations, whereby methods 4500-H^+ [27] and 3111 [28] were used in determining the two parameters, respectively. pH was determined using Orion pH meter model 811 supplied by Orion Research, Inc., Cambridge, Mass. Flame atomization on AA spectrophotometer model SOLAAR atomic absorption spectrophotometer with ASX-510 auto-sampler was used in an effort to determine chromium concentration with a lower detection limit of 0.1 mg L^{-1}.

All tests were run in duplicates with most in triplicates. The column adsorption tests were performed at a temperature of 22 ± 2 °C and covered five different Cr(VI) concentrations (0.5, 2, 6, 20, and 50 mg L^{-1}) at pH 4, with the first two concentrations being also tested at pH 5 and 6.

2.3 Batch adsorption tests

Batch adsorption tests were performed to determine related adsorption equilibria and kinetics for the tested AC. Batch tests were conducted at constant pH values, adsorbent concentration, and room temperature (22 ± 2 °C). Adsorbent concentration value was set at 4 g L^{-1}, and the pH selected was that determined from column tests to be the optimal for specific metal removal. 100 mL metal solutions were mixed with 0.4 g of pine-needle AC in 125-mL conical flasks under constant magnetic stirring at 150 rpm during the first 4 h after which it was reduced to 100 rpm until equilibrium was reached.

In selecting the pH values to be adopted in the experimental work, reference was made to the specific metal hydroxide solubility levels. Varied metal concentrations were selected for the metal to conform to the most common concentrations normally discharged in industrial wastewaters as reported by the US Federal Water Pollution Control Act (as amended through P.L. 107–303, November 27, 2002).

2.3.1 Adsorption isotherm

Three adsorption isotherm models were tested for the batch reactions which included the Langmuir, the Freundlich, and the Temkin models. The Langmuir model assumes that the adsorbed molecules form a monolayer and that adsorption can occur at a fixed number of adsorption sites and all of them being equivalent in adsorption abilities. Moreover, it assumes that every molecule has a constant enthalpy and sorption activation energy, meaning that all molecules have

equal affinity to all adsorption sites. The Langmuir isotherm is represented by the following equation:

$$q_e = \frac{q_{max} K_L C_e}{(1 + K_L C_e)} \quad (3)$$

where q_e is the amount of ions adsorbed at equilibrium (mg g^{-1}), q_{max} is the monolayer adsorption capacity of the adsorbent, C_e is the equilibrium concentration (mg L^{-1}), and K_L is the Langmuir adsorption constant (L mg^{-1}).

To evaluate the adsorption capacity for a particular range of adsorbate concentrations, Eq. 5 is linearized to read as follows:

$$\frac{C_e}{q_e} = \left(\frac{1}{q_{max}}\right) C_e + \left(\frac{1}{K_L q_{max}}\right). \quad (4)$$

The constants q_{max} and K_L are determined by plotting C_e/q_e versus C_e and determining the slope and equation of the resulting curve. Moreover, a dimensionless constant known as separation factor (R_L) can be calculated using the following equation:

$$R_L = \frac{1}{(1 + K_L C_0)}. \quad (5)$$

The R_L value indicates the adsorption nature to be either unfavorable ($R_L > 1$), linear ($R_L = 1$), favorable ($0 < R_L < 1$), or irreversible ($R_L = 0$) [29, 30].

The Freundlich model, which supports multilayer adsorption, agrees with the Langmuir model over moderate ranges of concentrations but differs at low and high concentrations. The Freundlich model applies better at low concentrations and is represented by the following equation:

$$q_e = K_F C_e^{1/n} \quad (6)$$

where K_F and n are constants related to the adsorption capacity and adsorption intensity, respectively. When linearized, the equation will take the following from:

$$\ln q_e = \ln K_F + \left(\frac{1}{n}\right) \ln C_e. \quad (7)$$

The values of K_F and n can be obtained from the intercept and slope of the linear line that results from a plot of $\ln q_e$ versus $\ln C_e$.

The Temkin model, considered to be the simplest of the models, was developed by considering the chemisorption of an absorbate onto the adsorbent [30, 31]. The Temkin isotherm equation is represented by:

$$q_e = \left[\left(\frac{RT}{b_T}\right) \ln C_e\right] + \left[\left(\frac{RT}{b_T}\right) \ln K_T\right] \quad (8)$$

where $\frac{RT}{b_T} = B$, $K_T = A$, R is the universal gas constant (8.3145 J $mol^{-1} K^{-1}$), T is the absolute temperature, in K, b_T is the variation of the adsorption energy (J mol^{-1}), K_T is the equilibrium binding constant (L g^{-1}), and A and B are constants.

By plotting q_e versus $\ln C_e$, a straight line is generated from which (RT/b_T) and K_T are determined from the slope and intercept of the line.

2.3.2 Adsorption kinetics

Pseudo-first-order and pseudo-second-order models were used in modeling adsorption kinetics. The respective linear forms of the model equations are presented by the following equations [23]:

$$\ln (q_e - q_t) = \ln q_e - k_1 t \quad (9)$$

and

$$\frac{t}{q_t} = \left(\frac{1}{k_2 q_e^2}\right) + \left(\frac{1}{q_e}\right) t \quad (10)$$

where q_t is the amount of ions adsorbed at time t (mg g^{-1}), k_1 and k_2 are the pseudo-first-order and pseudo-second-order model rate constants expressed in min^{-1} and g mg min^{-1}, respectively.

3 Results and discussion

3.1 Surface characteristics of pine-needle AC

Characterization of the produced pine-needle AC was performed by determining the parametric values based on analytical methods adopted from ASTM standards and reported in Table S1. ASTM classifies powdered activated carbon any AC that has a particle size predominately smaller than an 80-mesh sieve (0.177 mm opening). Particle size distribution of the pine-needle AC is presented in Table S2 complying with ASTM standards. Figure 1 shows the SEM for the micrograph of the pine-needle AC before and after the application of Cr(VI). Figure 1a shows a clear highly porous structure of the AC, while Fig. 1b shows a marked difference of the AC surface structure after the adsorption process with some pores that appear to have been occupied with an unidentified matter which might be chromium deposits and possibly solvent-induced morphological change [32]. Elemental analysis (Table 1) of the precursor and the AC indicate that carbon is the predominant element, followed by oxygen, which probably is present in functional groups on the surface of the AC. As shown in Table 2, the high silica content could be

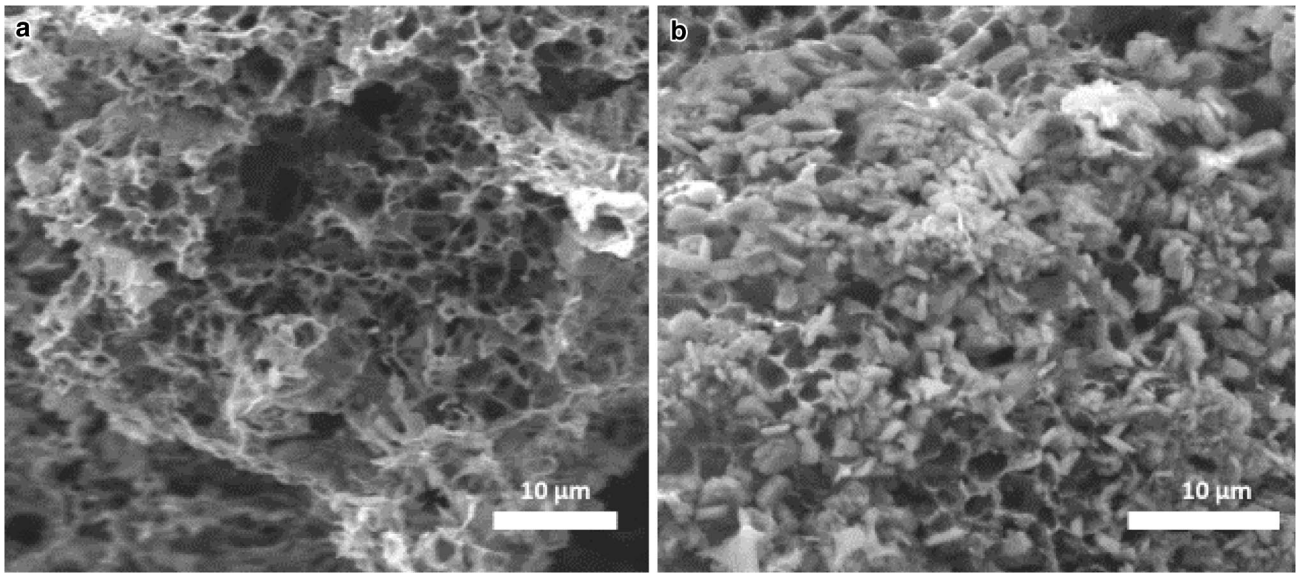

Fig. 1 SEM images of the pine-needle AC **a** before and **b** after Cr(VI) adsorption

Table 1 CHN elemental analysis on pine needles and pine-needle AC

	Element	C	H	N	O	S
% Weight	Pine needles	42.2	6	0.85	19.2	0.9
	Pine-needle AC	58.6	3.9	0.1	12.1	0.4

Table 2 Metals analysis on pine needles and pine-needle AC

Element	Pine needles	Pine-needle AC
Silica (mg/g Si)	8.5	3.9
Chlorides (mg/g Cl)	4.5	4
Sodium (mg/g Na)	25	14
Potassium (mg/g K)	18	82

responsible for the relatively high ash content detected in the pine-needle AC [33]. The potassium present could be attributed to residues resulting from the chemical activation step where KOH was used and possibly from the initial chemical ($K_2Cr_2O_7$) used in the preparation of the Cr(VI) solution.

The spectrum produced from the FT-IR is shown in Fig. 2. Peak characteristics are presented in Table S3 where it can be seen that the resulting functional groups corroborate results reported for several other types of AC [34, 35]. These groups will affect the pH of the AC, the point of zero charge (PZC), and the different reactions that may take place between the AC and the adsorbed molecules. The final versus the initial pHs are depicted in Fig. 3 where it can be seen that the PZC of the pine-needle AC is close to 3. This indicates that at pH values above 3, the pine-needle AC would be able to exchange cations, which among different pollutants would favor the removal of heavy metals that are present in the cationic form.

From the DTG curve presented in Fig. 4, it is noted that thermal decomposition of pine-needle AC takes place in three well-evident stages. The first loss extends between 50 and 149 °C attributed to loss of adsorbed $H_2O_{(l)}$ on the surface of the AC. The second and the third weight losses are weaker than the first occurring between 149–425 °C and 425–770 °C, respectively. These losses can be attributed to the presence of carbonyl groups on the AC surface.

3.2 Effect of Cr(VI) concentration and pH on adsorption capacities in column tests

The capacity of the pine-needle AC to adsorb Cr(VI) at pH values of 4, 5, and 6 and varying concentrations of 0.5 and 2 mg L^{-1} for the fixed-bed column tests are presented in Fig. 5a, b. Starting with an initial concentration of 0.5 mg L^{-1}, full breakthrough was achieved at 350 min and 100 min for the runs carried out under pH 5 and 6, respectively. A clear delay in breakthrough was reported when operating under pH 4 which was reached at 550 min. Upon increasing the concentration of Cr(IV) in the feed water to 2 mg L^{-1} under the same conditions, breakthrough

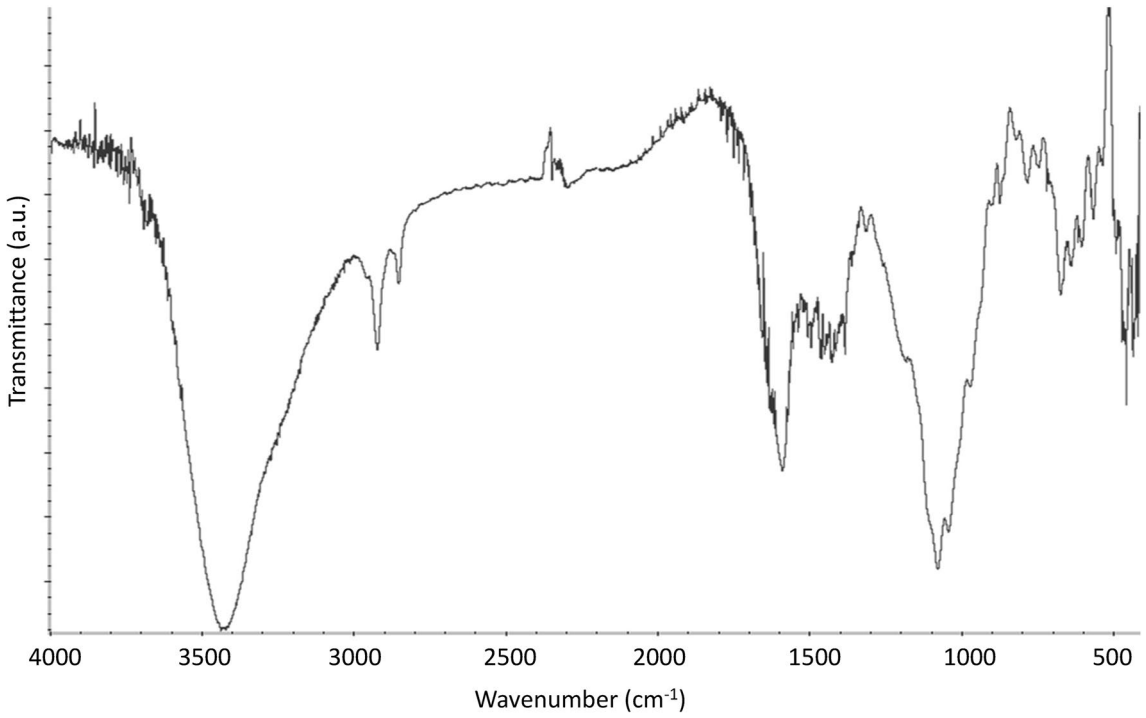

Fig. 2 FT-IR spectrum of pine-needle AC

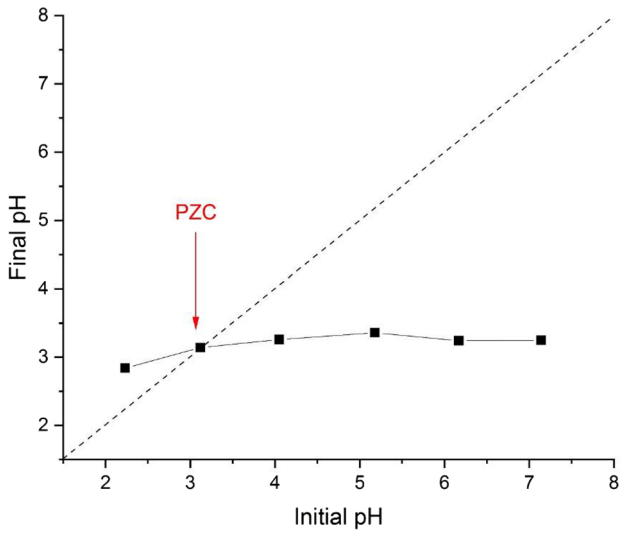

Fig. 3 Point of zero charge (PZC)

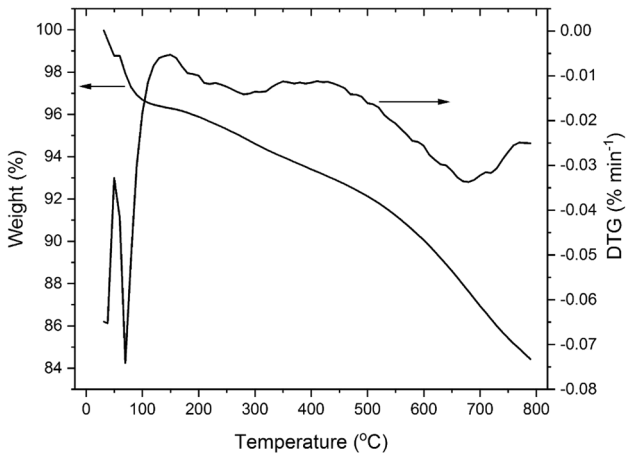

Fig. 4 TGA and DTG curves for pine-needle AC

was reached after 11 and 9 min when operating under pH 5 and 6, respectively. A further delay in breakthrough (580 min) was reported when operating under pH 4.

System pH affects the adsorption process in two ways, first by affecting the functional groups on the active sites of the AC and second by affecting the speciation of the metal ions in solution, i.e., adsorption of heavy metal ions onto AC. In the present study, the effect of pH on the removal capacity of the pine-needle AC is distinct. It is noted that the change in pH did not have a major effect on the surface functional groups of the AC. Consequently, the variation in removal capacity could be linked to the speciation of the metal ions in solution.

The resulting data on pH variation indicate that Cr(VI) is almost exclusively removed at low pH. The speciation diagram for Cr(VI) (Fig. 6 [36]) shows a clear difference in the distribution of the different species of Cr(VI) at different pH values. In the conducted experiments, the highest

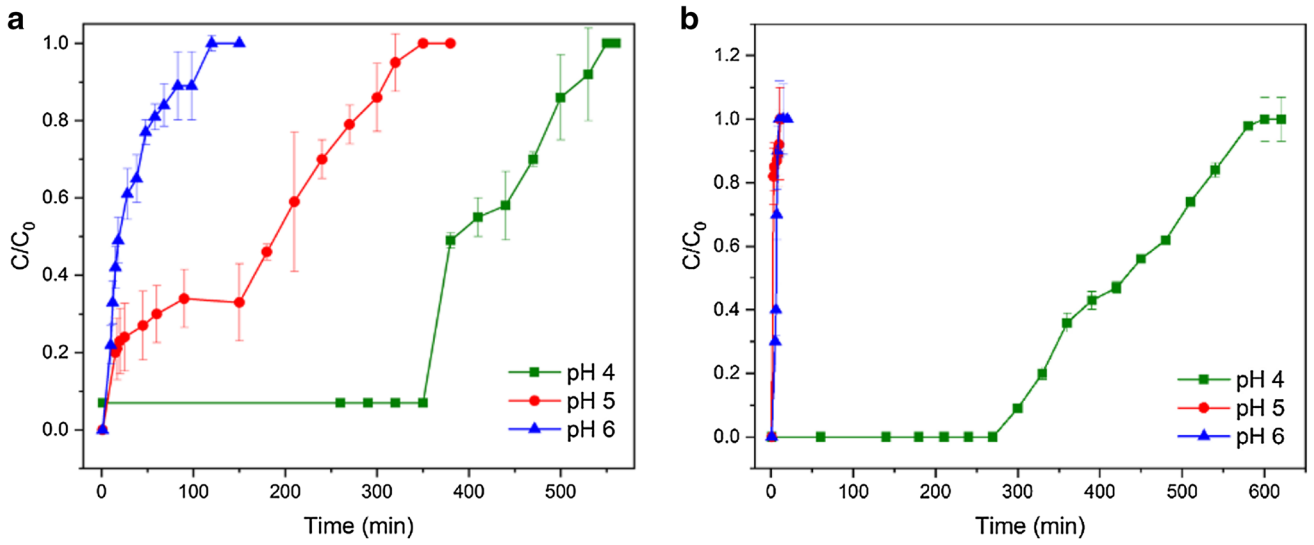

Fig. 5 Breakthrough curves for Cr(VI) removal at varying pH and initial concentrations of **a** 0.5 and **b** 2 mg L^{-1}

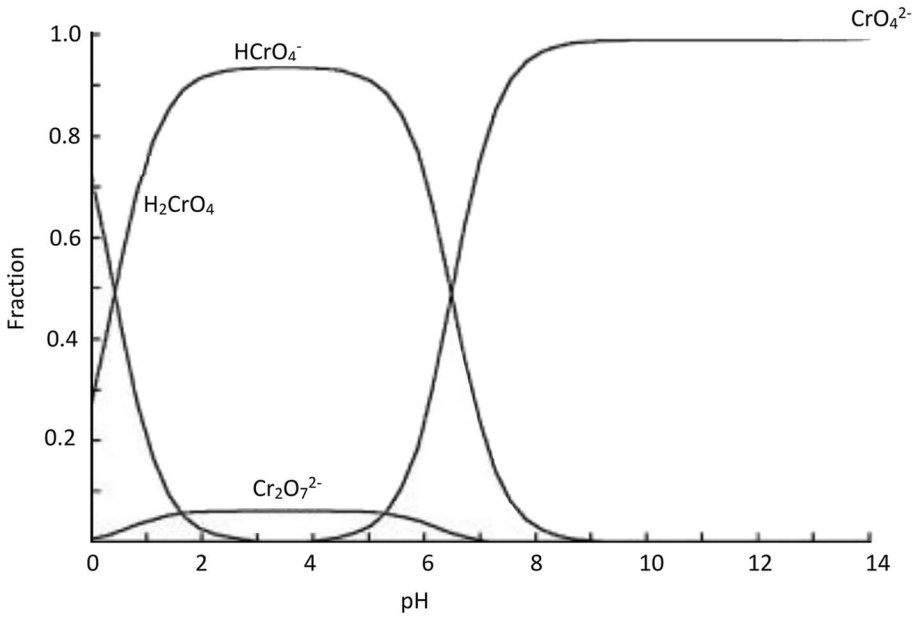

Fig. 6 Speciation diagram for Cr(VI)

adsorption of Cr(VI) took place, at pH 4, when the level of $HCrO_4^-$ was the highest and the level of CrO_4^{2-} was the lowest. Increasing the pH from 4 to 6 favors the formation of CrO_4^{2-} which is expected to result in a stronger electrostatic repulsion with the negative charge surface of the AC (PZC = 3.12). The decrease in adsorption capacity of the AC could thus be due to the electrostatic repulsion between the AC surface and the chromium ions according to the speciation diagram. In this context, it is to be noted that maximum adsorption should have occurred at a pH of 3, and however, a test at this pH was not conducted. Another possibility for this behavior could be attributed to the presence of the hydrogen atoms at low pH, which might introduce hydrogen bonding as a mechanism of removal. It should be noted that a number of researchers have noted a similar behavior and have speculated that the reduction in adsorption capacity at higher pH values may be due to competitive adsorption between chromate and hydroxyl ions.

Further testing was carried out under pH 4 which was determined to be the optimal condition for removal of Cr(IV). The breakthrough curves for Cr(IV) under pH 4 were fitted using traditional adsorption behavior. Models applied for this study were Bohart–Adams, Thomas, and Yoon–Nelson. Bohart and Adams [37] is based on the surface reaction theory and is considered to best describe

the initial parts of sorption breakthrough curves which is expressed as [38, 39]:

$$\ln\left(\frac{C_t}{C_o}\right) = k_{AB}C_0 t - k_{AB}N_0\frac{Z}{u_0} \tag{11}$$

where k_{AB} (L/mg min) is the Bohart mass transfer coefficient and C_o and C_t are influent and effluent concentrations, respectively. t (min) is the sample time, N_0 (mg/L) is the saturation concentration, U_0 (cm/min) is the linear velocity calculated by dividing the flow rate by the column cross-sectional area, and Z (cm) is the bed depth [40, 41]. The Thomas model [42] is the most general and widely used model for expressing the theoretical behavior of adsorption column performances. The model has the following form [43, 44]:

$$\ln\left(\frac{C_0}{C_t} - 1\right) = \frac{K_{Th}q_0 m}{Q} - K_{Th}C_0 t \tag{12}$$

where Q is the volumetric flow rate, K_{Th} is Thomas kinetic coefficient, t is the total flow time (min), and q_0 and m are the adsorption capacity and mass of the adsorbent, respectively. Yoon–Nelson model is a simpler model utilized for single component systems and is expressed as [45, 46]:

$$\ln\frac{C_t}{C_0 - C_t} = K_{YN}t - \tau K_{YN} \tag{13}$$

where K_{YN} is the rate constant, τ is time required for 50% adsorbate breakthrough, and t is time of the run. Applying the aforementioned models on experimental data, the values of each model parameters were determined and are presented in Table 3. Both Thomas and Bohart–Adams model fittings yielded R^2 values ranging from 0.81 to 0.97 indicating good linearity. Observed values of k_{AB} show a slight increase with increase in initial concentration which is in agreement with Guibal et al. [47] who stated that overall system kinetics may have been influenced by external mass transfer. Results indicate that K_{TH} decreases and q_0 increases with increased concentration. Yoon–Nelson model had the best R^2 value among the used models indicating that this model best describes the breakthrough. Yoon–Nelson parameters K_{YN} and τ showed a similar pattern to K_{TH} and q_0.

Using the formula by Ghribi and Chlendi [48], error analysis was carried out so as to determine the model that best describes the experimental data:

$$\delta = \sqrt{\frac{\sum\left(\frac{C}{Co}\right)_{cal} - \left(\frac{C}{Co}\right)_{exp}}{N}} \tag{14}$$

where N is the number of observations, $(C/Co)_{cal}$ and $(C/Co)_{exp}$ are the model obtained ratios of effluent to influent metal concentrations and the ratios obtained from experimental data, respectively. Table 4 depicts Yoon–Nelson model to best describe the data. In addition, the plots in Fig. 7 show that the predicted Thomas and Yoon–Nelson curves to be extremely close to experimental data and to each other.

It can be deduced that higher Cr(VI) removals are mostly effected at lower initial concentrations, with lower removals exercised at higher initial concentrations. The capacities of the AC, however, increase as the concentration increases to attain its maximum level at an initial concentration of 20 mg L^{-1} beyond which a decrease takes place at 50 mg L^{-1} to reach the range of the initial low-level capacities recorded for concentrations of 0.5–6 mg L^{-1}.

3.3 Adsorption isotherms

The batch adsorption experiments were conducted to determine the isotherms that best fit the adsorption process for

Table 4 Error values

Concentration (mg L^{-1})	Bohart and Adams (δ)	Thomas (δ)	Yoon and nelson (δ)
0.5	0.99	0.022	0.023
2	0.98	0.08	0.012
6	0.9	0.023	0.023
20	0.92	0.044	0.021
50	0.75	0.024	0.024

Table 3 Model parameters

Concentration (mg L^{-1})	Bohart and Adams			Thomas			Yoon and nelson		
	R^2	K_{AB} [L (mg min)$^{-1}$]	No (mg L^{-1})	R^2	K_{TH} [mL (min mg)$^{-1}$]	$q0$ (mg g^{-1})	R^2	K_{YN} (min^{-1})	τ (min)
0.5	0.89	0.0175	346.8	0.89	0.035	1.3	0.98	0.0014	215.5
2	0.97	0.02	384.5	0.97	0.01	5.8	0.82	0.0148	51.8
6	0.88	0.0203	48.4	0.88	0.003383	2.2	0.83	0.0348	5.9
20	0.85	0.023	131.3	0.85	0.00115	19.7	0.9	0.162	2.5
50	0.81	0.0198	126.2	0.81	0.000396	47.3	0.93	0.405	1.0

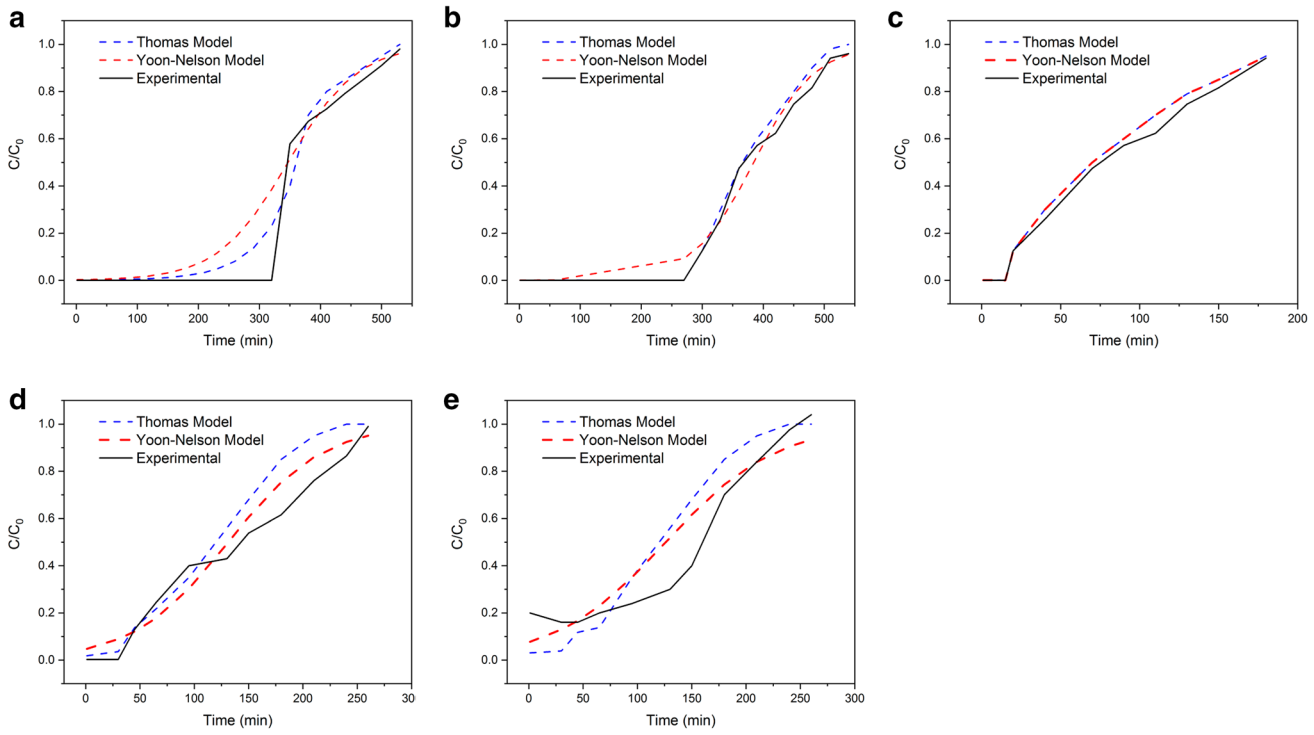

Fig. 7 Predictive vs experimental data at pH 4. **a** 0.5 mg L^{-1}, **b** 2 mg L^{-1}, **c** 6 mg L^{-1}, **d** 20 mg L^{-1}, and **e** 50 mg L^{-1}

the tested metal. The tests were performed taking account of the specific conditions that were deemed to have shown the best result for the specific metal. For adsorbate concentrations ranging between 5 and 200 mg L^{-1} the maximum adsorption capacity of 41.13 mg Cr(IV) per gram of AC was reported at pH 4.

Figure S2 and Table 5 show plots and calculated results, respectively, of the data fitting for the Langmuir, Freundlich, and Temkin models. Among the tested isotherm models, the results indicate that for Cr(VI) the Freundlich and the Temkin seem to best represent the adsorption data.

The separation factor (equilibrium parameter) R_L, which represents the essential characteristics of the Langmuir isotherm, has been found to vary between 0.78 and 0.99 for the different tested metal concentrations, i.e., between 0 and 1, which indicates that the adsorption is favorable [49]. As for the Freundlich adsorption isotherm, the results indicate that the calculated values for the adsorption capacity constant K_F were 3.412 while the n value is 1.413, which also represents favorable adsorption. It is to be noted that the correlation coefficient (R^2) recorded for the Freundlich isotherm (0.927) shows a better fit than that of the Langmuir model (0.853) and the Temkin model also shows a high correlation with R^2 equal to 0.953. The experimental results obtained for the adsorption isotherm show a good adsorption capacity (q_{max}) of 65.36 mg g^{-1}.

3.4 Adsorption kinetics

The rate kinetics of Cr(VI) adsorption on pine-needle AC analyzed from the linear plots for the pseudo-first- and pseudo-second-order equations (Figure S3) indicate better fit of the pseudo-second-order model with the experimental data compared to the first-order model. The result is supported by earlier findings [50–53]. Using intra-particle diffusion model, the root time dependence was determined based on the following equation [54]:

$$q_t = k_{id}\sqrt{T} + I \tag{15}$$

where q_t is the quantity of solute on the surface of the sorbent at time t (mg g^{-1}), kid the intra-particle diffusion rate constant [mg (g min 1/2)−1], t the time, and I is the

Table 5 Batch adsorption models

Metal	Langmuir parameters				Freundlich parameters			Temkin parameters		
	q_{max}	K_L	R_L	R^2	n	K_F	R^2	A	B	R^2
Cr(VI)	65.36	0.0446	0.78–0.99	0.853	1.413	3.412	0.927	1.01	5.081	0.953

Table 6 Intra-particle diffusion model parameters

Concentration (mg L^{-1})	R^2	k_{id}	I
0.5	1.00	0.34	7.83
2	0.72	0.69	19.06
6	0.92	3.25	45.54
20	0.92	10.33	189.30
50	0.71	23.31	439.06

intercept (mg g^{-1}). The calculated model parameters are given in Table 6, which indicates an increase in both k_{id} and I with increased Cr(IV) concentration. According to Rai et al. [55], the increase in the values of the parameters corresponds to the increase in boundary layer thickness which gives more importance to the surface adsorption as the rate limiting step. Additionally, the value of I indicates the involvement of some other mechanism in the process, which could be an indicator that chemisorption might be the mechanism responsible for the removal of Cr(VI) with pine-needle AC used as a sorbent.

3.5 Adsorption mechanism

Based on the results obtained, an evaluation of the adsorption mechanism of Cr(VI) is attempted herewith. The speciation of Cr(VI) at different solution pH values helps in determining the ionic state of its active functional groups [52, 56]. Gherasim et al. [36] showed that at pH between 2 and 6 Cr(VI) ions exist as $HCrO_4^-$ and $Cr_2O_7^{2-}$ species with $HCrO_4^-$ at its highest concentration and $Cr_2O_7^{2-}$ at its lowest (Fig. 6). Miretzky and Cirelli [57] reported that these species can be adsorbed to the protonated active sites of the adsorbent and that at pH values greater than 6 the adsorption of Cr(VI) is limited due to competition between the existing anionic species and OH^- for adsorption sites. Chen et al. [1] inferred that the possible removal mechanism of Cr(VI) could be due to the migration of Cr(VI) species ($HCrO_4^-$) to the positive charged adsorption sites mainly due to electrostatic driving forces and due to Cr(VI) being reduced to Cr(III) by contact with electron donor groups of the adsorbent surface [58]. It may also be added that with $HCrO_4^-$ being the governing species in the acidic range the presence of the hydrogen atoms might induce hydrogen bonding as a mechanism of removal [59].

3.6 Comparison of pine-needle adsorption capacities with other types of AC

A comparison of Cr(VI) adsorption capacities between the performance of several laboratory-prepared AC's and the pine-needle AC is presented in Table 7. For the purpose of

Table 7 Comparing Cr(VI) adsorption capacity of the pine-needle AC and other laboratory-prepared ACs

AC type	Capacity (mg g^{-1})	Experiment conditions	References
Cornelian cherry	q_{exp} = 59.4	pH = 1—Initial Cr(VI) = 300 mg L^{-1}	[60]
Apricot stone	q_{exp} = 58.86	pH = 1—Initial Cr(VI) = 300 mg L^{-1}	[60]
Almond shells	q_{exp} = 59.64	pH = 1—Initial Cr(VI) = 100 mg L^{-1}	[60]
Coconut shell	q_{max} = 11.51	pH = 2—Initial Cr(VI) = 100 mg L^{-1} AC dose = 2 g L^{-1}	[61]
Coconut fiber	q_{max} = 21.75	pH = 2—Initial Cr(VI) = 100 mg L^{-1} AC dose = 2 g L^{-1}	[61]
Oilpalm shell	q_{max} = 154	pH = 4—Initial Cr(VI) = 20 mg L^{-1} AC dose = 20 g L^{-1}	[62, 63]
Sugar waste	q_{max} = 41.2	pH = 5—Initial Cr(VI) = 44 mg L^{-1} AC dose = 5 g L^{-1}	[64]
Tuncbilek lignite	q_{max} = 33.9	pH = 2—Initial Cr(VI) = 500 mg L^{-1}	[65]
Coconut	q_{max} = 13.88	Initial Cr(VI) = 5–50 mg L^{-1}—AC dose = 2 g L^{-1}	[66]
Coal reject	q_{max} = 29.9	pH = 5	[3]
Hazelnut shell	q_{max} = 52.2	pH = 3	[3]
Fir wood	q_{exp} = 74.5	pH = 3	[3]
Modified corn stalks	q_{max} = 200	Initial Cr(VI) = 100–400 mg L^{-1}—AC dose 0.5—4 mg L^{-1}	[1]
Modified Bamboo charcoal	q_{max} = 35.7 (Fe MBC) q_{max} = 51.7 (Co–Fe–MBC)	pH = 5	[67]
Palm kernel shell	q_{max} = 125	Initial Cr(VI) = 10–100 mg L^{-1}	[68]
Mango kernel	q_{max} = 7.8	Initial Cr(VI) = 200–1000 mg L^{-1}	[4]
Green coconut shell	q_{max} = 22.96	Initial Cr(VI) = 10–100 mg L^{-1}—AC dose 2—10 mg L^{-1}	[69]
Almond shell	q_{max} = 195	Initial Cr(VI) = 50–1000 mg L^{-1}	[55]
Pine needle	q_{max} = 65.36 q_{exp} = 41.13	Batch run: pH = 4—Initial Cr(VI) 200 mg L^{-1}—AC dose = 4 g L^{-1}	Present study

this comparison, the optimal conditions and the highest achieved capacities are indicated.

It is noted from the results reported in Table 6 that pine-needle AC presents a relatively high adsorption capacity for Cr(VI) compared to other ACs reported in the literature.

4 Conclusions

KOH-activated pine-needle AC was examined as a sorbent for hexavalent chromium removal from aqueous solution. Results have indicated that maximum Cr(VI) adsorption is effected at relatively low pH solutions (in the range of 3–4) with appreciable adsorption reduction at higher pH values. This behavior is substantiated by the low pH_{PZC} (3.12) whereby increase in pH favors the formation of CrO_4^{-2} at the cost of $HCrO_4^-$ which results in a stronger electrostatic repulsion and thus reduced adsorption. The initial metal concentration of 20 mg L^{-1} resulted in optimal adsorption capacity when tested within an initial concentration range of 0.5–50 mg L^{-1}. It was deduced that adsorption isotherm exhibits Freundlich behavior, indicating multilayer adsorption. Following the pseudo-second-order adsorption kinetics revealed that chemisorption is the mechanism responsible for the removal of Cr(VI) using pine-needle AC. The measured and calculated maximum adsorption capacities of 41.13 mg g^{-1} and 65.36 mg g^{-1}, respectively, are considered quite effective compared to the capacities recorded for many other AC precursors. It is to be noted that the proposed precursor material is a feasible, effective, and sustainable alternative sorbent and widely available at a low cost.

Acknowledgements The authors acknowledge the Environmental Engineering Research Center at the American University of Beirut in providing its facilities for conducting the study. The authors would also like to acknowledge the reviewers for their comments, which lead to the enhancement of the quality of the manuscript.

Compliance with ethical standards

Conflict of interest The authors declare that they have no conflict of interest.

References

1. Chen S, Yue Q, Gao B, Li Q, Xu X, Fu K (2012) Adsorption of hexavalent chromium from aqueous solution by modified corn stalk: a fixed-bed column study. Bioresour Technol 113:114–120. https://doi.org/10.1016/j.biortech.2011.11.110
2. Cherdchoo W, Nithettham S, Charoenpanich J (2019) Removal of Cr(VI) from synthetic wastewater by adsorption onto coffee ground and mixed waste tea. Chemosphere 221:758–767. https://doi.org/10.1016/j.chemosphere.2019.01.100
3. Khezami L, Capart R (2005) Removal of chromium(VI) from aqueous solution by activated carbons: kinetic and equilibrium studies. J Hazard Mater 123(1):223–231. https://doi.org/10.1016/j.jhazmat.2005.04.012
4. Rai MK, Shahi G, Meena V, Meena R, Chakraborty S, Singh RS, Rai BN (2016) Removal of hexavalent chromium Cr(VI) using activated carbon prepared from mango kernel activated with H_3PO_4. Resour Eff Technol 2:S63–S70. https://doi.org/10.1016/j.reffit.2016.11.011
5. Zhang W, Qian L, Ouyang D, Chen Y, Han L, Chen M (2019) Effective removal of Cr(VI) by attapulgite-supported nanoscale zero-valent iron from aqueous solution: enhanced adsorption and crystallization. Chemosphere 221:683–692. https://doi.org/10.1016/j.chemosphere.2019.01.070
6. Itankar N, Patil Y (2014) Management of hexavalent chromium from industrial waste using low-cost waste biomass. Proc Soc Behav Sci 133:219–224. https://doi.org/10.1016/j.sbspro.2014.04.187
7. Sharma DC, Forster CF (1994) A preliminary examination into the adsorption of hexavalent chromium using low-cost adsorbents. Bioresour Technol 47(3):257–264. https://doi.org/10.1016/0960-8524(94)90189-9
8. Chakrabarti S, Mitra P, Banerjee P, Sarkar D (2014) Reduction of hexavalent chromium present in wastewater by steel wool in a continuous flow system. APCBEE Proced 10:59–63. https://doi.org/10.1016/j.apcbee.2014.10.016
9. Deng B, Stone AT (1996) Surface-catalyzed chromium(VI) reduction: reactivity comparisons of different organic reductants and different oxide surfaces. Environ Sci Technol 30(8):2484–2494. https://doi.org/10.1021/es950780p
10. Neagu V, Mikhalovsky S (2010) Removal of hexavalent chromium by new quaternized crosslinked poly(4-vinylpyridines). J Hazard Mater 183(1):533–540. https://doi.org/10.1016/j.jhazmat.2010.07.057
11. Kera NH, Bhaumik M, Pillay K, Ray SS, Maity A (2017) Selective removal of toxic Cr(VI) from aqueous solution by adsorption combined with reduction at a magnetic nanocomposite surface. J Colloid Interface Sci 503:214–228. https://doi.org/10.1016/j.jcis.2017.05.018
12. Thomas DH, Rohrer JS, Jackson PE, Pak T, Scott JN (2002) Determination of hexavalent chromium at the level of the california public health goal by ion chromatography. J Chromatogr A 956(1):255–259. https://doi.org/10.1016/S0021-9673(01)01506-0
13. MoE- L (1996) Standard for air and water quality. Leban Off J 45:3187
14. Zang Y, Yue Q, Kan Y, Zhang L, Gao B (2018) Research on adsorption of Cr(VI) by Poly-epichlorohydrin-dimethylamine (EPIDMA) modified weakly basic anion exchange resin D301. Ecotoxicol Environ Saf 161:467–473. https://doi.org/10.1016/j.ecoenv.2018.06.020
15. Hosseini-Bandegharaei A, Hosseini MS, Sarw-Ghadi M, Zowghi S, Hosseini E, Hosseini-Bandegharaei H (2010) Kinetics, equilibrium and thermodynamic study of Cr(VI) sorption into toluidine blue o-impregnated XAD-7 resin beads and its application for the treatment of wastewaters containing Cr(VI). Chem Eng J 160(1):190–198. https://doi.org/10.1016/j.cej.2010.03.040
16. Hu J, Chen G, Lo IMC (2005) Removal and recovery of Cr(VI) from wastewater by maghemite nanoparticles. Water Res 39(18):4528–4536. https://doi.org/10.1016/j.watres.2005.05.051
17. Kakavandi B, Kalantary RR, Farzadkia M, Mahvi AH, Esrafili A, Azari A, Yari AR, Javid AB (2014) Enhanced chromium (VI) removal using activated carbon modified by zero valent iron and silver bimetallic nanoparticles. J Environ Health Sci Eng 12(1):115. https://doi.org/10.1186/s40201-014-0115-5

18. Gupta VK, Rastogi A, Nayak A (2010) Adsorption studies on the removal of hexavalent chromium from aqueous solution using a low cost fertilizer industry waste material. J Colloid Interface Sci 342(1):135–141. https://doi.org/10.1016/j.jcis.2009.09.065
19. Ghaneian MT, Dehvari M, Jamshidi B (2013) A batch study of hexavalent chromium removal from synthetic wastewater using modified Russian knapweed flower powder. Int J Environ Health Eng 2(5):38–46
20. Chen S, Yue Q, Gao B, Li Q, Xu X (2011) Removal of Cr(VI) from aqueous solution using modified corn stalks: characteristic, equilibrium, kinetic and thermodynamic study. Chem Eng J 168(2):909–917. https://doi.org/10.1016/j.cej.2011.01.063
21. Wen X, Sun N, Yan C, Zhou S, Pang T (2018) Rapid removal of Cr(VI) ions by densely grafted corn stalk fibers: high adsorption capacity and excellent recyclable property. J Taiwan Inst Chem Eng 89:95–104. https://doi.org/10.1016/j.jtice.2018.04.021
22. Shawabkeh RA, Rockstraw DA, Bhada RK (2002) Copper and strontium adsorption by a novel carbon material manufactured from pecan shells. Carbon 40(5):781–786. https://doi.org/10.1016/S0008-6223(01)00198-1
23. Baccar R, Blánquez P, Bouzid J, Feki M, Sarrà M (2010) Equilibrium, thermodynamic and kinetic studies on adsorption of commercial dye by activated carbon derived from olive-waste cakes. Chem Eng J 165(2):457–464. https://doi.org/10.1016/j.cej.2010.09.033
24. Momčilović M, Purenović M, Bojić A, Zarubica A, Ranđelović M (2011) Removal of lead(II) ions from aqueous solutions by adsorption onto pine cone activated carbon. Desalination 276(1):53–59. https://doi.org/10.1016/j.desal.2011.03.013
25. Singh SR, Singh AP (2012) Treatment of water containing chromium (VI) using rice husk carbon as a new low cost adsorbent. Int J Environ Res 6(4):917–924
26. Appel C, Ma LQ, Dean Rhue R, Kennelley E (2003) Point of zero charge determination in soils and minerals via traditional methods and detection of electroacoustic mobility. Geoderma 113(1):77–93. https://doi.org/10.1016/S0016-7061(02)00316-6
27. Assessment of 17beta-estradiol removal from wastewater via abiotic and biotic routes and potential effects on food chain pathways.pdf
28. Oasis hlb rev.pdf
29. Aljeboree AM, Alshirifi AN, Alkaim AF (2017) Kinetics and equilibrium study for the adsorption of textile dyes on coconut shell activated carbon. Arab J Chem 10:S3381–S3393. https://doi.org/10.1016/j.arabjc.2014.01.020
30. Foo KY, Hameed BH (2010) Insights into the modeling of adsorption isotherm systems. Chem Eng J 156(1):2–10. https://doi.org/10.1016/j.cej.2009.09.013
31. Banerjee S, Chattopadhyaya MC (2017) Adsorption characteristics for the removal of a toxic dye, tartrazine from aqueous solutions by a low cost agricultural by-product. Arab J Chem 10:S1629–S1638. https://doi.org/10.1016/j.arabjc.2013.06.005
32. Albadarin AB, Mangwandi C, AaH A-M, Walker GM, Allen SJ, Ahmad MNM (2012) Kinetic and thermodynamics of chromium ions adsorption onto low-cost dolomite adsorbent. Chem Eng J 179:193–202. https://doi.org/10.1016/j.cej.2011.10.080
33. Rychlicki G, Terzyk AP, Majchrzycki W (1999) The effect of commercial carbon de-ashing on its thermal stability and porosity. J Chem Technol Biotechnol 74(4):329–336. https://doi.org/10.1002/(sici)1097-4660(199904)74:4%3c329:Aid-jctb36%3e3.0.Co;2-y
34. Moreno-Castilla C, Lopez-Ramon MV, Carrasco-Marin F (2000) Changes in surface chemistry of activated carbons by wet oxidation. Carbon 38:1995–2001
35. Shin S, Jang J, Yoon S-H, Mochida I (1997) A study of the effect of heat treatment on functional groups of pitch based activated carbon fiber using FTIR. Carbon 35:1739–1743
36. Gherasim C-V, Bourceanu G, Olariu R-I, Arsene C (2011) A novel polymer inclusion membrane applied in chromium(VI) separation from aqueous solutions. J Hazard Mater 197:244–253. https://doi.org/10.1016/j.jhazmat.2011.09.082
37. Bohart GS, Adams EQ (1920) Some aspects of the behavior of charcoal with respect to chlorine. J Am Chem Soc 42(3):523–544
38. Chu KH (2010) Fixed bed sorption: setting the record straight on the Bohart–Adams and Thomas models. J Hazard Mater 177(1):1006–1012. https://doi.org/10.1016/j.jhazmat.2010.01.019
39. Trgo M, Medvidović N, Peric J (2011) Application of mathematical empirical models to dynamic removal of lead on natural zeolite clinoptilolite in a fixed bed column. Indian J Chem Technol 18(2):123–131
40. Ahmad AA, Hameed BH (2010) Fixed-bed adsorption of reactive azo dye onto granular activated carbon prepared from waste. J Hazard Mater 175(1):298–303. https://doi.org/10.1016/j.jhazmat.2009.10.003
41. Marzbali MH, Esmaieli M (2017) Fixed bed adsorption of tetracycline on a mesoporous activated carbon: experimental study and neuro-fuzzy modeling. J Appl Res Technol 15(5):454–463. https://doi.org/10.1016/j.jart.2017.05.003
42. Rozada F, Otero M, García AI, Morán A (2007) Application in fixed-bed systems of adsorbents obtained from sewage sludge and discarded tyres. Dyes Pigm 72(1):47–56. https://doi.org/10.1016/j.dyepig.2005.07.016
43. Secor RM (1956) Mass-transfer operations. In: RE Treybal (ed) McGraw-Hill Book Company, Inc., New York (1955). 666 pages, $9.50. AIChE J 2(4):577–511D. https://doi.org/10.1002/aic.690020430
44. Karunarathne HDSS, Amarasinghe BMWPK (2013) Fixed bed adsorption column studies for the removal of aqueous phenol from activated carbon prepared from sugarcane bagasse. Energy Procedia 34:83–90. https://doi.org/10.1016/j.egypro.2013.06.736
45. Ayoob S, Gupta AK, Bhakat PB (2007) Analysis of breakthrough developments and modeling of fixed bed adsorption system for As(V) removal from water by modified calcined bauxite (MCB). Sep Purif Technol 52(3):430–438. https://doi.org/10.1016/j.seppur.2006.05.021
46. Yoon YH, Nelson JH (1984) Application of gas adsorption kinetics I A theoretical model for respirator cartridge service life. Am Ind Hyg Assoc J 45(8):509–516. https://doi.org/10.1080/15298668491400197
47. Guibal E, Lorenzelli R, Vincent T, Cloirec PL (1995) Application of silica gel to metal ion sorption: static and dynamic removal of uranyl ions. Environ Technol 16(2):101–114
48. Ghribi A, Chlendi M (2011) Modeling of fixed bed adsorption: application to the adsorption of an organic dye. Asian J Text 1:161. https://doi.org/10.3923/ajt.2011.161.171
49. McKay G, Blair HS, Gardner JR (1982) Adsorption of dyes on chitin. I. Equilibrium studies. J Appl Polym Sci 27(8):3043–3057. https://doi.org/10.1002/app.1982.070270827
50. Aliabadi M, Morshedzadeh K, Soheyli H (2006) Removal of hexavalent chromium from aqueous solution by lignocellulosic solid wastes. Int J Environ Sci Technol 3(3):321–325. https://doi.org/10.1007/bf03325940
51. Hossain MA, Kumita M, Michigami Y, Mori S (2005) Optimization of parameters for Cr(VI) adsorption on used black tea leaves. Adsorption 11(5):561–568. https://doi.org/10.1007/s10450-005-5613-4

52. Ho Y-S (2006) Review of second-order models for adsorption systems. J Hazard Mater 136(3):681–689. https://doi.org/10.1016/j.jhazmat.2005.12.043
53. Nagy B, Mânzatu C, Măicăneanu A, Indolean C, Barbu-Tudoran L, Majdik C (2017) Linear and nonlinear regression analysis for heavy metals removal using Agaricus bisporus macrofungus. Arab J Chem 10:S3569–S3579. https://doi.org/10.1016/j.arabjc.2014.03.004
54. Weber W, Morris J (1962) Advances in water pollution research. In: Proceedings of the first international conference on water pollution research. Pergamon Press, Oxford, p. 231
55. Rai MK, Giri BS, Nath Y, Bajaj H, Soni S, Singh RP, Singh RS, Rai BN (2018) Adsorption of hexavalent chromium from aqueous solution by activated carbon prepared from almond shell: kinetics, equilibrium and thermodynamics study. J Water Suppl Res Technol Aqua 67(8):724–737. https://doi.org/10.2166/aqua.2018.047
56. López-García M, Lodeiro P, Barriada JL, Herrero R, Sastre de Vicente ME (2010) Reduction of Cr(VI) levels in solution using bracken fern biomass: batch and column studies. Chem Eng J 165(2):517–523. https://doi.org/10.1016/j.cej.2010.09.058
57. Miretzky P, Cirelli AF (2010) Cr(VI) and Cr(III) removal from aqueous solution by raw and modified lignocellulosic materials: a review. J Hazard Mater 180(1):1–19. https://doi.org/10.1016/j.jhazmat.2010.04.060
58. Brunauer S, Emmett PH, Teller E (1938) Adsorption of gases in multimolecular layers. J Am Chem Soc 60(2):309–319
59. Franz M, Arafat HA, Pinto NG (2000) Effect of chemical surface heterogeneity on the adsorption mechanism of dissolved aromatics on activated carbon. Carbon 38(13):1807–1819. https://doi.org/10.1016/S0008-6223(00)00012-9
60. Demirbas EK, Kobya M, Senturk E, Ozkan T (2004) Adsorption kinetics for the removal of chromium (VI) from aqueous solutions on the activated carbons prepared from agricultural wastes. Water SA 30(4):533–539
61. Mohan D, Singh KP, Singh VK (2005) Removal of hexavalent chromium from aqueous solution using low-cost activated carbons derived from agricultural waste materials and activated carbon fabric cloth. Ind Eng Chem Res 44(4):1027–1042. https://doi.org/10.1021/ie0400898
62. Saifuddin MN, Kumaran P (2005) Removal of heavy metal from industrial wastewater using chitosan coated oil palm shell charcoal. Electron J Biotechnol 8:43–53
63. Saifuddin NM, Palanisamy K (2005) Removal of heavy metal from industrial wastewater using chitosan coated oil palm shell charcoal. Electron J Biotechnol. https://doi.org/10.2225/vol8-issue1-fulltext-7
64. Fahim NF, Barsoum BN, Eid AE, Khalil MS (2006) Removal of chromium(III) from tannery wastewater using activated carbon from sugar industrial waste. J Hazard Mater 136(2):303–309. https://doi.org/10.1016/j.jhazmat.2005.12.014
65. Yavuz R, Orbak İ, Karatepe N (2006) Factors affecting the adsorption of chromium(VI) on activated carbon. J Environ Sci Health Part A 41(9):1967–1980. https://doi.org/10.1080/10934520600779265
66. Liu SX, Chen X, Chen XY, Liu ZF, Wang HL (2007) Activated carbon with excellent chromium(VI) adsorption performance prepared by acid–base surface modification. J Hazard Mater 141(1):315–319. https://doi.org/10.1016/j.jhazmat.2006.07.006
67. Wang W, Wang X, Wang X, Yang L, Wu Z, Xia S, Zhao J (2013) Cr(VI) removal from aqueous solution with bamboo charcoal chemically modified by iron and cobalt with the assistance of microwave. J Environ Sci 25(9):1726–1735. https://doi.org/10.1016/S1001-0742(12)60247-2
68. Razavi Mehr M, Fekri MH, Omidali F, Eftekhari N, Akbari-adergani B (2019) Removal of chromium (VI) from wastewater by palm kernel shell-based on a green method. J Chem Health Risks 9(1):75–86. https://doi.org/10.22034/jchr.2019.664165
69. Kumar S, Meikap BC (2014) Removal of chromium(VI) from waste water by using adsorbent prepared from green coconut shell. Desalin Water Treat 52(16–18):3122–3132. https://doi.org/10.1080/19443994.2013.801796